Phase behavior of gradient copolymers

Aleksij Aksimentiev and Robert Hołyst

Citation: The Journal of Chemical Physics **111**, 2329 (1999); doi: 10.1063/1.479504
View online: http://dx.doi.org/10.1063/1.479504
View Table of Contents: http://scitation.aip.org/content/aip/journal/jcp/111/5?ver=pdfcov
Published by the AIP Publishing

Phase behavior of gradient copolymers

Aleksij Aksimentiev[a] and Robert Hołyst
Institute of Physical Chemistry and College of Science, Polish Academy of Sciences, Kasprzaka 44/52, 01-224 Warsaw, Poland

(Received 24 March 1999; accepted 3 May 1999)

Phase properties of gradient *AB* copolymer melts which consist of chains with the specified chemical distribution of *A* and *B* monomers have been studied within the Landau–Ginzburg model. All the melts with the linear distribution of the monomers exhibit only a direct continuous phase transition from disordered to the lamellar phase. The hexagonal, body-centered-cubic, double-gyroid (G), and lamellar-ordered structures have been found in the melts with the monotonic but nonlinear distribution of the monomers. The *G* structure has been also found in the gradient copolymer melts with the distribution function of monomers similar to the $A-B-A$ triblock copolymers. © *1999 American Institute of Physics.* [S0021-9606(99)50129-3]

I. INTRODUCTION

During the last two decades a large variety of ordered mesophases has been predicted and observed with the characteristic size of 50–5000 Å in complex systems such as surfactant solutions,[1–3] copolymer melts,[4–7] and liquid crystals.[8] The Landau–Ginzburg (LG) formalism[9] is often used to describe the ordering phenomena on this mesoscopic length scale. In this framework, a phase behavior of copolymer melts is determined by an index of polymerization of copolymer chains, *N*, a temperature dependent. Flory–Huggins interaction parameter, χ, and the chemical and geometrical architecture of the copolymer chains. In particular, one can design the phase behavior of a real copolymer melt by changing the architecture of chains. Here, we study this problem within the LG model. We concentrate on linear *AB* chains with various chemical distributions of monomers along the chain.

The simplest copolymer system is a diblock *AB* copolymer melt. It is formed by chains which consist of two blocks of distinct homopolymers joined together. One can expect the following types of ordering in such a system:[4,7,10–17] the lamellar mesophase (LAM); hexagonally packed cylinders (HEX); spheres arranged at the sites of a body-centered cubic (bcc) lattice (BCC); bi-continuous double-gyroid structure with $Ia\bar{3}d$ space group symmetry (G). Some other structures have also been studied: bicontinuous double-diamond structure with $Pn\bar{3}m$ space group symmetry (OBDD); hexagonally modulated lamellae (HML), and hexagonally perforated layers (HPL). Some of these structures have been found to be unstable in certain approaches.[16,18] Experimentally it has been found that the OBDD phase does not exist in the block copolymer system[19] and that the previously found OBDD phase was nothing more than the misidentified gyroid phase.[19] Recent experiments[20] showed that the HPL phase does exist but is not stable. The evidence of the HML phase is very weak and the theoretical studies[21] suggest that the experimental results concerning possible HML phase may be explained by the fluctuations of the lamellar phase. The three classical ordered phases—LAM, bcc, and HEX—have been also found in a triblock *ABA* copolymer melt.[22–24]

Another type of copolymer systems is *AB* random copolymer melts.[25–27] They are produced by a polymerization reaction in a medium which contains two different types of monomers.[28] The architecture of these chains is conditioned by reaction rates and can be conveniently described by a probability matrix. For example, the conditional probability that an *A*-type monomer is followed by a *B*-type monomer in the chain is given by the element p_{BA} of this matrix. If the polymerization process takes place under the steady-state conditions, the elements of the matrix p_{XY} do not depend on the position of the monomers in the chain. A quenched disordered architecture of such a chain is determined by the average composition of, say, *A*-type monomers and a certain combination of two elements of the matrix p_{XY}. It was shown[26,27,29] that LAM, HEX, and bcc mesophases could appear in the random or multiblock copolymer melts.

Here, we consider a copolymer melt which has been produced by the polymerization reaction under the non-steady-state conditions. We assume the ideal situation in which reaction rates can be precisely controlled by the change of external parameters. Additionally, we assume that the characteristic time at which a new monomer is joined to the chain during the polymerization process is comparable with the time needed by the reaction rates to adapt to the change of the external conditions. Even in this case, the chains could not be identical at the monomer length scale, but would have the same distribution of the monomers over a larger (a few monomers) length scale. The architecture of these chains can be described by a distribution function.[30] The melt of the linear *AB* copolymer chains with a specified distribution of the monomers along the chains we will call here a gradient copolymer melt. According to this definition, all known block copolymer melts are particular cases of a gradient copolymer melt. For example, the architecture of the diblock copolymer chain corresponds to the architecture of a gradient copolymer chain with the Heaveside step distribution function.

[a]Electronic mail: alek@saka.ichf.edu.pl

In this work, we are mainly concerned with the phase behavior of a gradient copolymer melt. As could be seen from the example of a diblock copolymer melt, some features of the phase diagram crucially depend on the concrete realization of the LG model. Within the mean-field approach, the only three ordered phases[4,22,31]—LAM, HEX, and bcc—can be found using a main-harmonic approximation for the density profiles. Including the second harmonic allows us to consider more complex structures[12,18,32] (e.g., gyroid bicontinuous phase). Marques and Cates have speculated[33] that, in addition to the classical structures, two further structures [face-centered cubic (fcc) and square (SQ) structures] could stabilize. However, a quantitatively correct phase diagram can be obtained only by including a large number of higher harmonics.[34] From the other side, the fluctuation corrections which are not included in the mean-field theory could also change the phase diagram.[10,12] But, since we are interested mostly in the qualitative description of the phase behavior, we can define our minimal model within the Leibler mean-field theory with the two-harmonics representation of the density profiles.

A consideration of the gradient copolymers allows us to investigate immediate correlations between the distribution of monomers in a chain and the phase properties of a copolymer melt. It is also possible to relate an existence of ordered phases and succession of their appearance to the average composition of monomers in the sample and deviation of the monomer distribution from the uniform distribution. Modifying the monomer distribution of copolymer chains, we could specify such an architecture, which would stabilize a structure of a given morphology. In particular, we are interested in such melts which could self-organize into stable structures with complex topologies.

The rest of the paper is organized as follows: in the next section we specify the Leibler theory for the gradient copolymer melt and specify briefly the ordered structures considered in this paper. In Sec. III we describe phase properties of different gradient copolymer melts. The paper ends with a short discussion of the obtained results.

II. THEORY

We consider a mixture of n polymer molecules inside a volume V. Each of the molecules consists of N_A monomers of type A and N_B monomers of type B. Let $\{A\}$ and $\{B\}$ denote the positions of the monomers of type A and type B consequently in the chain. For example, a chain *AABABAA* would have the following position of $\{A\}=\{1,2,4,6,7\}$ and $\{B\}=\{3,5\}$. We assume that all chains are identical (we could also assume the different sets $\{A\}$ and $\{B\}$ for each of the chains with the same averaged monomer distribution function). Location of the ith monomer in the αth molecule is given by the position vector $\mathbf{r}_i^\alpha$. Orientation of a bond connecting monomers i and $i-1$ is given by $\mathbf{u}_i^\alpha=\mathbf{r}_i^\alpha-\mathbf{r}_{i-1}^\alpha$. To describe the flexible polymer, the chain model is used, in which the monomers are described as being joined by freely rotating bonds of fixed length l (we assume the same bond lengths for $A-A$, $A-B$, and $B-B$ bonds). The information that N monomers are connected to form a chain is specified by the spatial distribution function $W(\mathbf{r})$

$$W(\mathbf{r})=\prod_{i=1}^{N}\frac{\delta(|\mathbf{u}_i|-l)}{4\pi l^2}, \tag{1}$$

where $\delta(x)$ is the Dirac delta function, and $N=N_A+N_B$ is the index of polymerization.

The interaction Hamiltonian with the specified short-range interactions between the monomers is given by the following expression:[35,36]

$$H_I=\frac{\rho_0}{k_BT}\int\frac{d\mathbf{q}}{(2\pi)^3}\left[\frac{1}{2}w_{AA}|\hat{\phi}_A(\mathbf{q})|^2+\frac{1}{2}w_{BB}|\hat{\phi}_B(\mathbf{q})|^2+w_{AB}\hat{\phi}_A(\mathbf{q})\hat{\phi}_{\mathbf{B}}(-\mathbf{q})\right], \tag{2}$$

where $\rho_0=n(N_A+N_B)/V$ is the number density of monomers in the system. $\hat{\phi}_A(\mathbf{q})$ and $\hat{\phi}_B(\mathbf{q})$ are the Fourier transforms of the microscopic concentration operators,

$$\hat{\phi}_A(\mathbf{q})=\frac{1}{\rho_0}\sum_{\alpha=1}^{n}\sum_{i=\{A\}}\exp(\mathbf{q}\mathbf{r}_i^\alpha),$$

$$\hat{\phi}_B(\mathbf{q})=\frac{1}{\rho_0}\sum_{\alpha=1}^{n}\sum_{i=\{B\}}\exp(\mathbf{q}\mathbf{r}_i^\alpha). \tag{3}$$

This part of the Hamiltonian leads to a microphase separation of copolymer melts providing that $w_{AA}+w_{BB}-2w_{AB}=-2k_BT\chi<0$. Here, χ is the usual Flory–Huggins parameter. The origin of the interaction parameters w_{AA}, w_{BB}, w_{AB} is the van der Waals attraction between the monomers and the steric repulsive forces. Additionally, the steric repulsive forces are included in the form of a constraint of incompressibility.

Now, we can specify our mesoscopic model. Let $\phi_A(\mathbf{q})$ and $\phi_B(\mathbf{q})$ be the values of the microscopic concentration operators averaged over some mesoscopic volume. The conditional partition function, $Z(\phi_\gamma)$ $(\gamma=A,B)$, is the partition function for the system subject to the constraint that the microscopic operators $\hat{\phi}_\gamma(\mathbf{q})$ $(\gamma=A,B)$ are fixed at some prescribed values[37] of $\phi_\gamma(\mathbf{q})$, i.e.,

$$Z(\phi_\gamma)=N_0\prod_{\alpha=1}^{n}\int D\mathbf{r}^\alpha\, W(\mathbf{r}^\alpha)\times\prod_{\gamma=A,B}\delta[\phi_\gamma(\mathbf{q})-\hat{\phi}_\gamma(\mathbf{q})]\exp\left(-\frac{H_I}{k_BT}\right). \tag{4}$$

Here, N_0 is a constant, $D\mathbf{r}^\alpha$ denotes the measure $1/V\, d\mathbf{r}_0^\alpha\, d\mathbf{r}_1^\alpha,\ldots,d\mathbf{r}_N^\alpha$, the interaction Hamiltonian H_I is given by Eq. (2), and $W(\mathbf{r}^\alpha)$ is the spatial distribution function, Eq. (1).

For infinitely small χ there is no interaction in the system and the chains are mixed uniformly. The average values of $\phi_A(\mathbf{q})$ and $\phi_B(\mathbf{q})$ are equal to f and $1-f$, respectively, where f is the composition of the A-type monomers: $f=N_A/(N_A+N_B)$. To describe the different phases in our system, we specify an order parameter $\Psi(\mathbf{r})$ as[4]

$$\Psi(\mathbf{r})=\langle(1-f)\phi_A(\mathbf{r})-f\phi_B(\mathbf{r})\rangle, \tag{5}$$

where $\langle\cdots\rangle$ denotes a thermal average. $\Psi(\mathbf{r})$ has a vanishing value at any point in the isotropic phase, and is nonzero in the ordered phase. We assume that our system is incompressible, i.e.,

$$\phi_A(\mathbf{r})+\phi_B(\mathbf{r})=1, \tag{6}$$

so,

$$\Psi(\mathbf{r})=\langle\phi_A(\mathbf{r})-f\rangle. \tag{7}$$

It was shown[38,39] that our partition function, $Z(\phi_\gamma)$, could be rewritten as follows:

$$Z[\Psi]=\exp\left\{-\sum_{n=2}^{\infty}\frac{1}{n!}\int\frac{d\mathbf{q}_1}{(2\pi)^3}\cdots\int\frac{d\mathbf{q}_n}{(2\pi)^3}\Gamma_n(\mathbf{q}_1,\ldots,\mathbf{q}_n)\times\delta(\mathbf{q}_1+\cdots+\mathbf{q}_n)\Psi(-\mathbf{q}_1)\cdots\Psi(-\mathbf{q}_n)\right\}, \tag{8}$$

where the vertex functions Γ_n for $n>2$ are known functions arising from the ideal chain conformations and the interaction Hamiltonian, H_I, is included only in Γ_2; $\Psi(\mathbf{q})$ is a Fourier transform of $\Psi(\mathbf{r})$. The LG free energy (in the mean-field approach), $F[\Psi]$, is given by

$$F[\Psi]=-k_BT\ln Z[\Psi]. \tag{9}$$

This expansion of the free energy in powers of the order parameter, Ψ, is usually restricted to the fourth order. Hence, the LG free energy has the following form:[4,35]

$$F[\Psi]=\sum_{n=2}^{4}\frac{1}{n}\int\frac{d\mathbf{q}_1}{(2\pi)^3}\cdots\int\frac{d\mathbf{q}_n}{(2\pi)^3}\Gamma_n(\mathbf{q}_1,\ldots,\mathbf{q}_n)\times\delta(\mathbf{q}_1+\cdots+\mathbf{q}_n)\Psi(-\mathbf{q}_1)\cdots\Psi(-\mathbf{q}_n). \tag{10}$$

The LG free energy depends on the architecture of the copolymer chains through the vertex functions $\Gamma_n(\mathbf{q}_1,\ldots,\mathbf{q}_n)$. They are related to the momenta $S_{i,\ldots,j}=\langle\phi_i(\mathbf{q}_1)\cdots\phi_j(q_n)\rangle_0$ $(i,j=A,B)$ by the well-known formulas[4,40] which are reproduced in the Appendix. Let us calculate $\langle\phi_A(\mathbf{q}_1)\phi_B(\mathbf{q}_2)\rangle_0$

$$\langle\phi_A(\mathbf{q}_1)\phi_B(\mathbf{q}_2)\rangle_0=\frac{1}{\rho_0^2}\prod_{\alpha=1}^{n}\prod_{\beta=1}^{n}\int D\mathbf{r}^\alpha D\mathbf{r}^\beta W[\mathbf{r}^\alpha]W[\mathbf{r}^\beta]\times\sum_{a_1,a_2=1}^{n}\sum_{i=\{A\}}\sum_{j=\{B\}}\exp[\mathbf{q}_1\mathbf{r}_i^{a_1}+\mathbf{q}_2\mathbf{r}_j^{a_2}]. \tag{11}$$

We are interested only in that part of Eq. (11) which is proportional to $\delta(\mathbf{q}_1+\mathbf{q}_2)$. performing the integral over $\Pi_{\alpha=1}^{n}\Pi_{\beta=1}^{n}D\mathbf{r}^\alpha D\mathbf{r}^\beta$ gives[4,41]

$$\langle\phi_A(\mathbf{q}_1)\phi_B(\mathbf{q}_2)\rangle_0=\delta(\mathbf{q}_1+\mathbf{q}_2)\frac{n}{\rho_0^2}\sum_{i=\{A\}}\sum_{j=\{B\}}\prod_{s=1}^{N}\times\frac{\sin l[\mathbf{q}_1\theta(i-s)+\mathbf{q}_2\theta(j-s)]}{l[\mathbf{q}_1\theta(i-s)+\mathbf{q}_2\theta(j-s)]}, \tag{12}$$

where $\theta(i-s)$ is the Heaveside step function. Now, we can replace summation $\Sigma_{i=\{A\}}$ and $\Sigma_{j=\{B\}}$ by the integration with a monomer distribution function $g(x)$ or $1-g(x)$, i.e.,

$$\sum_{i=\{A\}}\cdots\rightarrow N\int_0^1\cdots g(x)dx, \tag{13}$$

$$\sum_{j=\{B\}}\cdots\rightarrow N\int_0^1\cdots[1-g(x)]dx. \tag{14}$$

The monomer distribution function $g(x)$ gives a probability to find a monomer of type A at the distance $x\cdot N$ from the beginning of the chain. It should obviously satisfy the following conditions: $0<g(x)<1$ for every x. The composition, f, is given by

$$f=\int_0^1 g(x)dx. \tag{15}$$

The phase properties of the melt should be irrelevant to the following transformations of $g(x)$:

$$g(x)\rightarrow g(1-x), \tag{16}$$

$$g(x)\rightarrow 1-g(x). \tag{17}$$

Finally, using an approximative relation

$$\frac{\sin l\mathbf{q}[\theta(i-s)-\theta(j-s)]}{l\mathbf{q}[\theta(i-s)-\theta(j-s)]}\approx\exp(-[l\mathbf{q}(\theta(i-s)-\theta(j-s))]^2/3!) \tag{18}$$

valid for $l\mathbf{q}\ll 1$ (let us remind that $l\mathbf{q}\sqrt{N/6}$ is of order of unity), one can obtain

$$\langle\phi_A(\mathbf{q}_1)\phi_B(\mathbf{q}_2)\rangle_0=\delta(\mathbf{q}_1+\mathbf{q}_2)\frac{nN^2}{\rho_0^2}\int_0^1 dx\int_0^1 dy\, g(x)[1-g(y)]\times\exp\left\{-\frac{Nl^2}{6}\int_0^1 ds[\mathbf{q}_1\theta(x-s)+\mathbf{q}_2\theta(y-s)]^2\right\}. \tag{19}$$

The higher momenta can be evaluated in the similar way.

The order parameter $\Psi(\mathbf{r})$ in the ordered phase which is characterized by the set $\{\mathbf{Q}_{k,m}\}$ of the wave vectors in the reciprocal space can be expanded as

$$\Psi(\mathbf{r})=\sum_{m=1}^{\infty}\frac{1}{\sqrt{n_m}}A_m\sum_{k=1}^{n_m}\{\exp[i(\mathbf{Q}_{k,m}\mathbf{r}+\phi_{k,m})]+cc\}, \tag{20}$$

where A_m and $\phi_{k,m}$ are amplitudes and phases of this expansion in the ordered phase: m numbers the shells, and n_m is a number of wave vectors in the mth shell. Their equilibrium values are determined by the minimization of the free energy, $F[\Psi(\mathbf{r})]$, with respect to A_m and $\phi_{k,m}$ with additional constraints imposed on $\phi_{k,m}$ by the symmetry group of the ordered phase. The ordered phase with the smallest free energy for a given χN is the stable one.

In this work we restrict the infinite expansion in Eq. (20) to the second shell. The LG free energy [Eq. (10)] in the second harmonic approximation is written as follows:

$$F(A_1,A_2)=\Gamma_2(q_1,-q_1)A_1^2+\Gamma_2(q_2,-q_2)A_2^2 + \frac{1}{3!}\left(\frac{A_1^3}{n_1\sqrt{n_1}}G^{(3)}_{111}+\frac{A_2^3}{n_2\sqrt{n_2}}G^{(3)}_{222}+\frac{A_1^2A_2}{n_1\sqrt{n_2}} \times G^{(3)}_{112}+\frac{A_1A_2^2}{n_2\sqrt{n_1}}G^{(3)}_{122}\right)+\frac{1}{4!}\left(\frac{A_1^4}{n_1^2}G^{(4)}_{1111} + \frac{A_2^4}{n_2^2}G^{(4)}_{2222}+\frac{A_1^3A_2}{n_1\sqrt{n_1n_2}}G^{(4)}_{1112}+\frac{A_1^2A_2^2}{n_1n_2}G^{(4)}_{1122} + \frac{A_1A_2^3}{n_2\sqrt{n_1n_2}}G^{(4)}_{1222}\right), \tag{21}$$

where q_1 and q_2 are the absolute values of the first and second shell wave vectors,

$$G^{(3)}_{xyz}=\sum_{i=1}^{2n_x}{}' \sum_{j=1}^{2n_y}{}' \sum_{k=1}^{2n_z}{}' \Gamma_3(\mathbf{Q}_{i,x},\mathbf{Q}_{j,y},\mathbf{Q}_{k,z}) \times\delta(\mathbf{Q}_{i,x}+\mathbf{Q}_{j,y}+\mathbf{Q}_{k,z}) \times\exp[i(\phi_{i,x}+\phi_{j,y}+\phi_{k,z})], \tag{22}$$

$$G^{(4)}_{xyzp}=\sum_{i=1}^{2n_x}{}' \sum_{j=1}^{2n_y}{}' \sum_{k=1}^{2n_z}{}' \sum_{l=1}^{2n_p}{}' \Gamma_4(\mathbf{Q}_{i,x},\mathbf{Q}_{j,y},\mathbf{Q}_{k,z},\mathbf{Q}_{l,p}) \times\delta(\mathbf{Q}_{i,x}+\mathbf{Q}_{j,y}+\mathbf{Q}_{k,z}+\mathbf{Q}_{l,p}) \times\exp[i(\phi_{i,x}+\phi_{j,y}+\phi_{k,z}+\phi_{l,p})]. \tag{23}$$

Here, $\Sigma_{i=1}^{2n_x}{}'$ denotes the sum over the all wave vectors $\mathbf{Q}_{i,x}$ and phases $\phi_{i,x}$ $(i=1,...,n_x)$ which are taken with both signs in the xth shell $(x,y,z,p=1,2)$. The second-order term $\Gamma_2(\mathbf{q}-\mathbf{q})$ in Eq. (10) is proportional to the inverse of the scattering intensity which has a maximum at a certain wave vector q^*. For a special value of χN the scattering intensity diverges at this wave vector. This is the so-called spinodal point. In the mean-field approximation, we neglect a possible shift [12,42] of q^* and assume that the main harmonic of the ordered phase occurs exactly at q^*. Using a definition of the spinodal point, we have for $q_1=q^*$

$$\Gamma_2(q_1,-q_1)=2N(\chi_{\rm sp}-\chi),$$
$$\Gamma_2(q_2,-q_2)=2N(\chi_{\rm sec}-\chi), \tag{24}$$

where

$$N\chi_{\rm sec}=\Gamma_2(q_2,-q_2)|_{\chi=0}. \tag{25}$$

In order to check this assumption, we performed a minimization procedure which included a minimization over q^* for several points of the phase diagram. Obtained results were always close to the results of the minimization with fixed q^*. Thus, we suppose that the absolute values of the first shell wave vectors are equal to the absolute value of the peak position wave vector in the scattering intensity, $q_1=q^*$. However, the scattering intensity always has a finite width which leads to a finite contribution to the LG free energy from Fourier components with $q>q^*$. These are the ''harmonic corrections'' [33] which are taken into account in the theory by considering the contributions with $q\leqslant\sqrt{2}q^*$. In this case, only the second shell corrections appear in the LG free energy. We could not use only a one-shell representation of the ordered phases since some of the complex ordered structures would not be distinguished in the first shell approximation. For example, the bcc and OBDD structures have the same first shell. In addition, nontrivial modulations of the ordered phases could be obtained by varying the amplitudes A_1 and A_2 of their two-shell representation. In Fig. 1 and Fig. 2, two structures with the same first and second shells which correspond to the $Ia\bar{3}d$ symmetry group are shown. The first structure is obtained by setting different signs for A_1 and A_2 and represents a double-gyroid structure

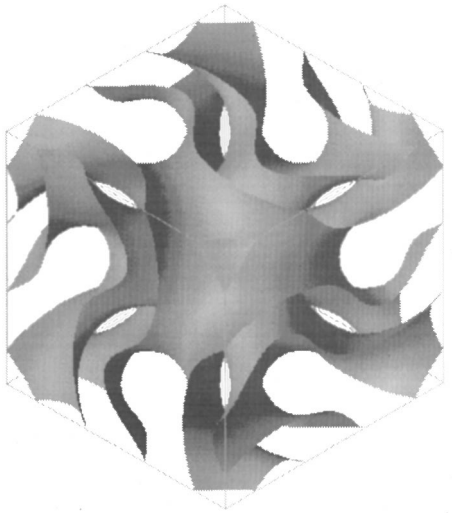

FIG. 1. The bicontinuous double-gyroid structure formed by the copolymer melts (one unit cell). The surfaces represent the interfaces between *A*-rich and *B*-rich domains, i.e., $\phi_A(\mathbf{r})=f$, where f is the average composition of the melt. This figure has been obtained considering the first and second shell of the structure with $Ia\bar{3}d$ symmetry group. The amplitudes $A_1=0.20$ and $A_2=-0.05$. The genus of this structure is 5 for each surface.

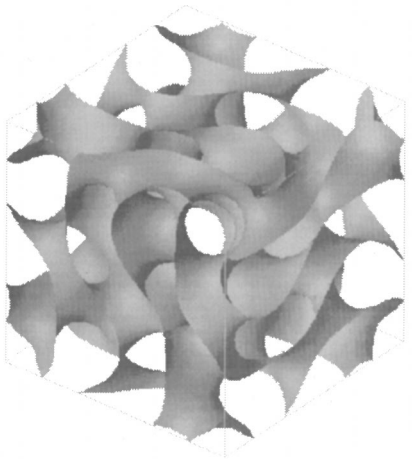

FIG. 2. This figure shows the structure which has been modeled by the first and second shell of the structure with $Ia\bar{3}d$ symmetry group. The amplitudes $A_1=0.20$ and $A_2=0.05$ and the genus of this structure is 25. The surfaces on this figure represent the interfaces between *A*-rich and *B*-rich domains.

with genus[43] equal to 5 for each surface in a unit cell. The second structure corresponds to A_1 and A_2 of the same signs. The genus of this structure is 25.

The following structures are considered in the paper:

(i) a lamellar structure.[4] It is formed by the layers with the excess concentration of the *A*-type or *B*-type monomers. They are arranged one after another in a certain direction (e.g., *Z*-axis). The distance between the nearest same type lamellae is a lamellar period given by $2\pi/q^*$. This structure is well defined by its first shell and the absolute value of the second shell wave vectors $q_2=2q^*>\sqrt{2}q^*$. Therefore, the second shell corrections are not considered.

(ii) a hexagonal structure.[4] It is formed by the cylinders with the excess concentration of, say, *A*-type monomers arranged on a 2-D honeycomb lattice in the matrix of the polymer with the excess concentration of *B*-type monomers. The second shell corrections with $q_2=\sqrt{3}q_1$ are not considered.

(iii) a square lattice 2-D structure.[4,33] This structure has been found to be stable for a certain class of model systems. The ratio of the absolute values of the second and first shell wave vectors $q_2/q_1=\sqrt{2}$.

(iv) a simple cubic structure[4,12,33] (SC). In this structure, the domains with the excess concentration are arranged at the sites of a simple cubic lattice. $q_2/q_1=\sqrt{2}$.

(v) a bcc structure.[4,31] This structure has a symmetry of $Im\bar{3}m$ space group.[44] It could be formed by the spherical domains arranged at the sites of a bcc lattice. Bicontinuous structures with $Im\bar{3}m$ space group has been also observed in surfactant solutions[45,43] and in plant cells.[46] $q_2/q_1=\sqrt{2}$.

(vi) a fcc structure.[4,12,33] The domains are arranged at the sites of a fcc lattice. $q_2/q_1=\sqrt{4/3}$.

(vii) a bicontinuous double-gyroid structure.[14,15,17,32] This structure has a symmetry of $Ia\bar{3}d$ space group.[44] An example of such a structure in given in Fig. 1. Two continuous surfaces in Fig. 1 show the points of the average concentration of *A*-type monomers $\phi(\mathbf{r})=f$, i.e., interfaces between the *A*-rich and *B*-rich domains $q_2/q_1=\sqrt{4/3}$.

(viii) a bicontinuous double-diamond structure.[11,12,14,18] This structure has a symmetry of $Pn\bar{3}m$ space group[44] and consists of two channels with the excess of *A*-type monomers in a continuous matrix with the excess of *B*-type monomers. Each of these channels exhibits diamond-cubic symmetry. $q_2/q_1=\sqrt{3/2}$.

(ix) HPL and HML structures.[12,13,17,18] These structures can be described by the superposition of a lamellar and hexagonal ordering. For example, the ordering in *XY* plane can be described by the first shell of the hexagonal structure: $\mathbf{Q}_{1,1}=[1,0,0]$; $\mathbf{Q}_{2,1}=[-1/2,\sqrt{3}/2,0]$; $\mathbf{Q}_{3,1}=[-1/2,-\sqrt{3}/2,0]$, while the second shell corresponds to the lamellar ordering in *Z* direction with $\mathbf{Q}_{1,2}=[0,0,d]$ $(1<d<\sqrt{2})$. Varying the amplitudes A_1 and A_2, different HPL or HML structures can be obtained. We also consider the HPL and HML structures, for which lamellar ordering is described by the first shell and hexagonal ordering—by the second shell.

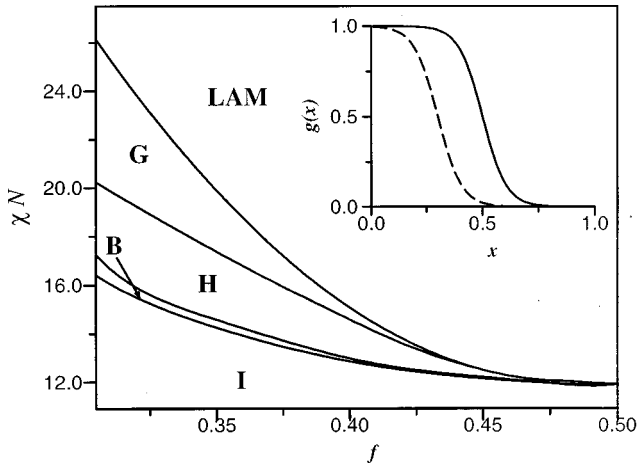

FIG. 3. The phase diagram of the gradient copolymer melt with the distribution functions $g(x)=\frac{1}{2}(1-\tanh(c_1\pi(x-f_0))$ shown on the insert of this figure for $c_1=3$, $f_0=0.5$ (solid line), and $f_0=0.3$ (dashed line). x_i gives the position of ith monomer from the end of the chain in the units of the linear chain length. χ is the Flory–Huggins interaction parameter, N is a polymerization index, f is the composition ($f=\int_0^1 g(x)dx$). Here, **I** denotes an isotropic, H-hexagonal, B-bcc, G-double gyroid (see Fig. 1), L-lamellar phases.

Coefficients $G^{(3)}_{111}, G^{(4)}_{1111}$, etc. for all these structures are given in the Appendix.

III. RESULTS

In order to compute the phase diagram of a gradient copolymer melt, one should first specify the distribution function $g(x)$. Then, the momenta S_{ij}, S_{ijl}, and S_{ijlk} needed to calculate coefficients $G^{(3)}_{xyz}$ and $G^{(4)}_{xyzp}$ have to be evaluated for each of the considered structures. After that, a minimization procedure is applied to the function $F(A_1,A_2)$ [Eq. (21)] with respect to the amplitudes A_1,A_2 for each value of χN. Evaluation of $G^{(3)}_{xyz}$ and $G^{(4)}_{xyzp}$ involves a 3-D and 4-D integration, which can be performed only numerically.

The first system under our consideration in the melt of copolymer chains with a distribution of the monomers along the chains similar to a diblock copolymer chain architecture. The distribution function, $g(x)$, of such a chain is

$$g(x)=\tfrac{1}{2}(1-\tanh(c_1\pi(x-f_0)), \tag{26}$$

where c_1 and f_0 determine a sharpness and position of the ''interface'' between the blocks of *A* and *B* monomers. The distribution function $q(x)$ is shown in the insert of Fig. 3 for $c_1=3$, $f_0=0.5$ (solid line), and $f_0=0.3$ (dashed line). In the limit of $c_1\to\infty$, the diblock architecture is recovered. Changing f_0 one can shift a position at which $g(x)=0.5$ and model an asymmetric diblock copolymer chain. The composition f in this case equals f_0.

The phase properties of such a melt are similar to the phase properties of a diblock copolymer melt and are summarized in a phase diagram (see Fig. 3). Four ordered morphologies has been found: bcc, HEX, G, and LAM. A

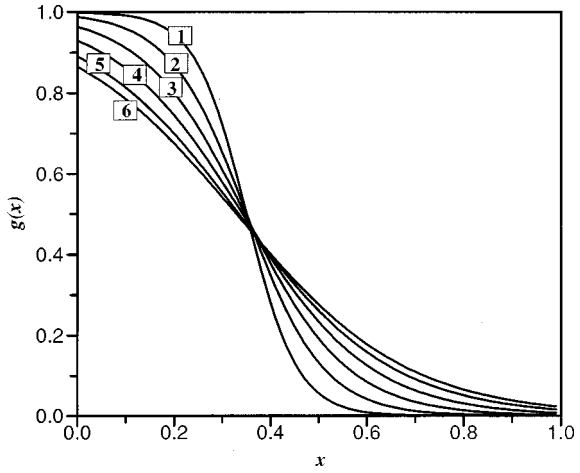

FIG. 4. The distribution functions $g(x)=\frac{1}{2}(1-\tanh(c_1\pi(x-f_0))$ with $f_0=3.5$ and $c_1=3,2,1.5,1.2,1,0.9$ used in the calculation of the phase diagrams shown in Fig. 5. Each of the distribution functions 1–6 corresponds to the same composition $f=0.35$. The G structure was found for distribution functions 1–5. For the melt with the distribution function 6, the G structure is not stable. As the architecture of the chains changes from the diblock architecture (point 1) to the architecture with nearly linear distribution of the monomers (point 6), q^* decreases. However, this decrease is small (about 5%).

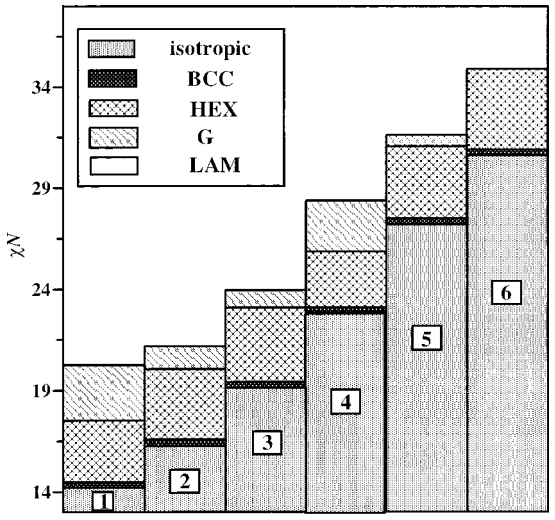

FIG. 5. The one-dimensional phase diagrams of the gradient copolymer melts ($f=0.35$) with the distribution functions $g(x)$ shown in Fig. 5. Please note that the G structure disappears for the nearly linear distribution function (function 6 in Fig. 5).

double-gyroid structure appears in the melt with the composition $f<0.44$. In this case, the phase transformations in the system caused by increasing χN take place in the following order: isotropic phase (I)→bcc→HEX→G→LAM. In the nearly symmetric melt ($f>0.44$), the order is as follows (I)→bcc→HEX→LAM. The phase diagram of this melt differs slightly from the phase diagrams of a diblock copolymer melt by a small shift of all the transition lines in Fig. 3 towards the higher values of χN. For example, a transition point of a symmetric diblock copolymer melt from I to LAM phase is $\chi N=10.495$ while in our case this transition happens at $\chi N=11.906$. The peak position wave vector in the scattering intensity, q^*, is also shifted to the smaller values. This shift is about 3%. A diffuse boundary between the blocks of A and B monomers in the chains causes the ordering with a larger characteristic length than in the diblock copolymer melt.

Next, we fix the composition of the melt at $f=0.35$ and vary parameter c_1 in Eq. (26) to change the shape of the distribution function as it is shown in Fig. 4. For each of the distribution functions (1–6 in Fig. 4) we compute the phase diagram of the melt. In Fig. 5, the one-dimensional phase diagrams (f is fixed) for each of the distribution functions are presented. The shape of the distribution function deviates more from the step-like one as the transition points are shifted more to the higher values of χN. This is consistent with a more general observation that the temperatures of the phase transitions of a copolymer melt decrease when monomers of different type in the chains are mixed more. In a completely random copolymer melt there is no ordering at all. One can observe that the double-gyroid structure disappears for nearly linear distribution functions (curve 6 in Fig. 4). For exactly linear distribution of the monomers in the chains $g(x)=C_2x$, only lamellar ordering is observed. Here, we vary C_2 from 0.6 to 1, which corresponds to the range of the compositions from 0.3 to 0.5. The peak position wave vectors in the scattering intensity for the distribution functions 1–6 are 1.936, 1.912, 1.894, 1.881, 1.873, and 1.866, consequently, and for the linear distribution $g(x)=0.7x$ with $f=0.35$ $q^*=1.842$ (q^* is given in units of $1/l(N/6)^{-1/2}$, where l is the Kuhn length). As the architecture of the chains changes from the diblock architecture to the architecture with linear distribution of the monomers, q^* decreases, which leads to the increase of the characteristic length of ordering. However, this increase is small (about 5%).

In order to investigate the phase behavior of the gradient copolymer melt with the monotonic distribution of the monomers along the chains, we consider the following class of distribution functions:

$$g(x)=x^{\gamma}, \tag{27}$$

with

$$f=\frac{1}{1+\gamma}. \tag{28}$$

We change the power γ in $g(x)$ from 0.25 up to 4 to cover the range of the compositions from 0.2 up to 0.8. The shapes of the distribution function $g(x)=x^{\gamma}$ for $\gamma=0.25$, 0.5, 1, 2, and 4 are given in the insert of Fig. 6. The phase diagram of such melts (shown in Fig. 6) is described in terms of the composition, f, and Flory–Huggins interaction parameter, χN. There is no symmetry of the phase diagram due to the interchange of f with $1-f$, since the left-hand side of the diagram has been calculated using distribution functions $g(x)=x^{\gamma}$ with $\gamma>1$ while the right-hand side has been calculated using $g(x)=x^{\gamma}$ with $\gamma<1$. Two distribution functions, $g_1(x)=x^{\gamma}$ and $g_2(x)=x^{1/\gamma}$ with corresponding compositions f_1 and f_2 such that $f_1+f_2=1$, describe significantly different monomer distributions. In Fig. 7 the distribution functions $g_1(x)$ and $1-g_2(x)$ [which is equivalent to $g_2(x)$] for $\gamma=2$ and $\gamma=4$ are shown as solid [$g_1(x)$]

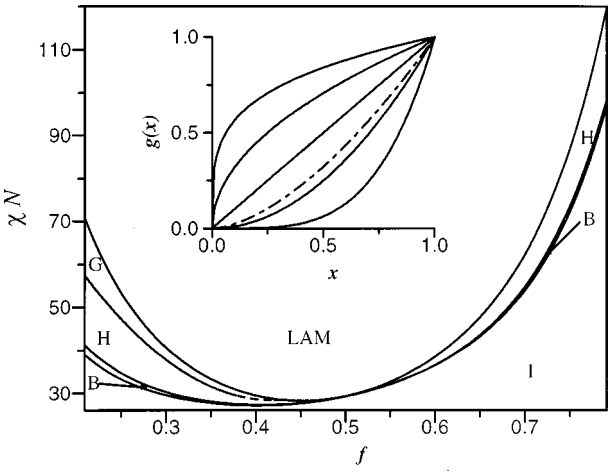

FIG. 6. The phase diagram of the gradient copolymer melt with the distribution functions $g(x)=x^{\gamma}$ shown in the insert of this figure. The left-hand side of the phase diagram has been calculated for $g(x)=x^{\gamma}$, $\gamma>1$ ($f<0.5$), while the right-hand side has been calculated for $g(x)=x^{\gamma}$, $\gamma<1$ ($f>0.5$). The part of the H–G phase boundary which is shown as dashed line has been obtained by interpolation. In the insert, the distribution functions with $\gamma=0.25$, 0.5, 1, 2, 4 are shown (from top to bottom) as solid lines. For all the distribution functions below the dot–dashed line (i.e., increasing γ), we find the stable G structure (see also Fig. 7).

and dashed $[g_2(x)]$ lines. One can see that the distribution functions given by the solid lines have large regions of high probability to find a *B*-type monomer in the chain (at x between 0 and 0.3). The shapes of the dashed lines resemble straight lines. The dot–dashed line in Fig. 7 presents the distribution function $g(x)=x^{\gamma}$, $\gamma>1$ which corresponds to the composition $f=0.37$. The G structure always appears between HEX and LAM phases at the phase diagram of these melts with the smaller compositions, $f<0.37$. The transition line between HEX and G phases is shown as a solid line in Fig. 6. In the interval of compositions $0.37<f<0.43$, the differences in the energies of the HEX and G phases are very

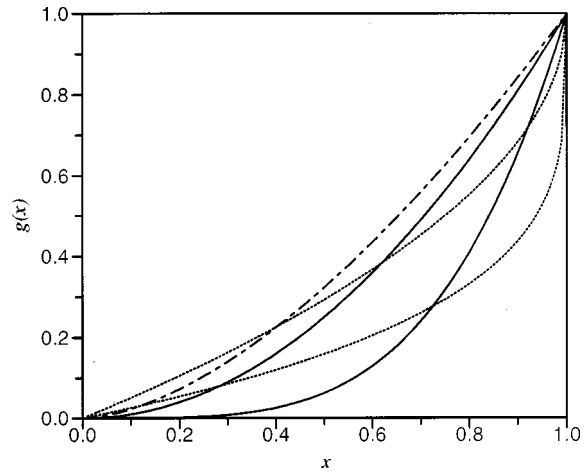

FIG. 7. The distribution functions $g(x)=x^{\gamma}$ with $\gamma=2$, 4 shown from top to bottom as solid lines and the distribution functions $g(x)=1-x^{\gamma}$ with $\gamma=0.5$, 0.25 shown from top to bottom as dotted lines. The distribution functions with the same composition have different chain architecture and G structures appear only for the distribution functions shown as solid lines. The dot–dashed line represents that distribution function for which the G structures appear on the phase diagram (see also Fig. 6).

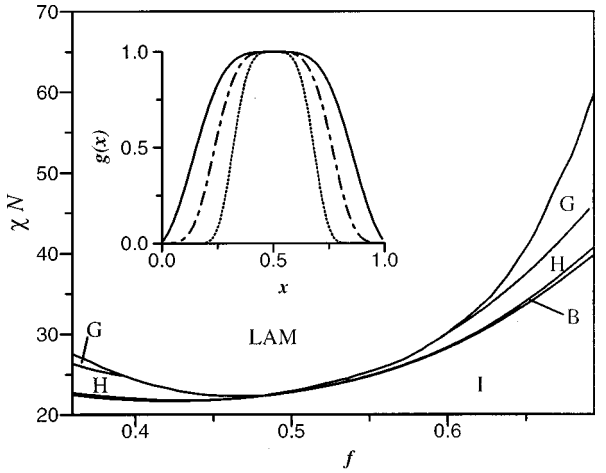

FIG. 8. The phase diagram of the gradient copolymer melt with the distribution functions $g(x)=\exp[-(c_3\pi(x-x_0))^4]$ shown in the insert of this figure for $c_3=1.6$ (dotted line), $c_3=1.2$ (dot–dashed line), and $c_3=0.85$ (solid line). These melts are analogous to the triblock $B-A-B$ copolymer melts. The G structure appears in the melts with nonsymmetric compositions ($f<0.4$, $f>0.6$).

small and appearance of the G phase depends very much on γ. The peak wave vector q^* of the melts with $\gamma>1$ in $g(x)$ exhibits a similar dependence on f as in a diblock copolymer melt. However, this dependence is shifted to the lower values due to the mixed arrangement of the different-type monomers along the chains. In contrast, the values of q^* of the melts with $\gamma<1$ in $g(x)$ do not depend on f at all. One can note that the diblock copolymer melts and the melts with $g(x)=x^{\gamma}$ and $\gamma>1$ have similar phase behaviors (existence of the G structure) and the peak wave-vector dependences on the composition.

The last class of the systems considered in this work has the following distribution functions:

$$g(x)=\exp[-(c_3\pi(x-x_0))^4]. \tag{29}$$

These distribution functions are similar to a triblock $B-A-B$ distribution. The length of block A is controlled by c_3 and is centered at x_0. The shapes of these distribution functions for different values of c_3 are shown in the insert of Fig. 8. Block B is always centered at $x_0=0.5$ (symmetric case). The phase diagram of such melts is shown in Fig. 8. In addition to the three classical mesophases (LAM, HEX, bcc), a G structure has been found. It appears again in the melts with nonsymmetric compositions ($f<0.4$, $f>0.6$). The phase diagram is not symmetric since the melts with the analogous compositions (f and $1-f$) have a completely different chain architecture. Contrary to the melts considered previously, for $f=0.5$ not only lamellar-ordered morphology could exist in these systems. However, there is another special point $f\sim0.49$ at which the phase transition from disordered phase takes place directly to the lamellar structure (analogous to the point $f=0.5$ in the diblock copolymers). The region of the stability of the G structure has a bigger width for that architecture which is specified with a larger center block A. The peak wave-vector position q^* in the scattering intensity has significantly bigger values (q^* is about 2.6) in comparison to the peak position exhibited by the diblock melts. The

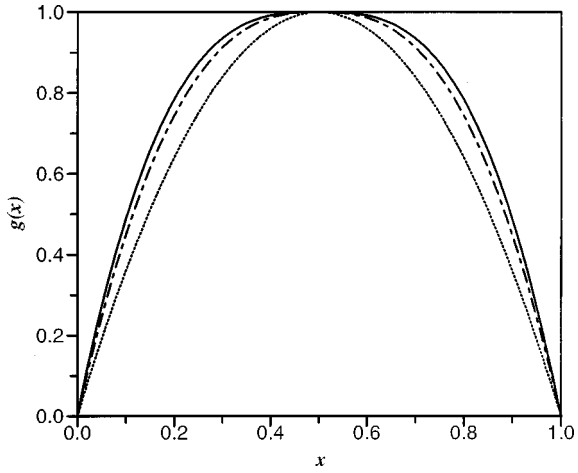

FIG. 9. The distribution functions $g(x)=(2(x-0.5))^{\beta}$ with $\beta=2$ (dotted line), $\beta=8/3$ (dot–dashed line), and $\beta=3$ (solid line) used to model the asymmetric triblock copolymer melts. The phase diagrams of these melts are shown in Fig. 10. The G structure has been found for all of these distribution functions.

distance between the domains of *B* monomers is smaller for the architecture with a shorter central block of *A* monomers. When the length of the central block is comparable with the total length of the shorter blocks the further increase of this length does not lead to the change of the peak wave-vector position.

The more asymmetric melts have been investigated using the distribution functions shown in Fig. 9. They correspond to the functions

$$g(x)=(2(x-0.5))^{\beta}, \tag{30}$$

with $\beta=2$ (dashed line, $f=2/3$), $\beta=8/3$ (dot–dashed line $f=0.7272$), and $\beta=3$ (dotted line, $f=0.75$). The G structure has been found in all of these melts. Their phase diagrams are shown in Fig. 10. They are in accordance with the interpolate continuation of the phase diagram shown in Fig. 8. In the case of more asymmetric melts ($f>0.75$), the differences between G and HPL (or HML) structures in their energies become undistinguished within our approach. The

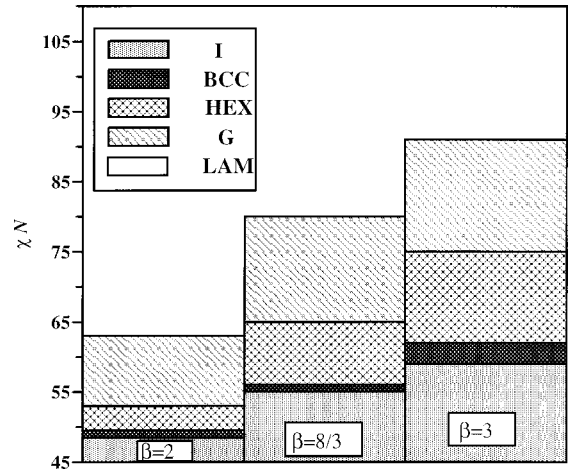

FIG. 10. The phase diagrams of the gradient copolymer melts with the distribution functions $g(x)=(2(x-0.5))^{\beta}$ shown in Fig. 9.

other scenario of the phase transformations in these systems which competes with the I–bcc–HEX–G–LAM transitions is I–bcc–HEX–HPL–HML–LAM phase transformations. The HPL structure has the period of lamellar ordering *d* 1.05 times greater than its hexagonal period, and the HML structure has the period of lamellar ordering *d* 1.05 times smaller than its hexagonal period.

IV. SUMMARY AND CONCLUSION

We have considered the phase properties of different gradient copolymer melts. All of the considered systems exhibit a disordered phase at high temperatures ($\chi\to 0$) and a stable lamellar phase at low temperatures ($\chi\to\infty$). There are three different scenarios of the phase transformations in our systems. The first one corresponds to the direct continuous transition from disordered to the lamellar phase. It has been found that symmetric composition of the melt, $f=0.5$, is not a necessary condition of such transformation. In addition to the diblock and triblock copolymers,[22] the gradient copolymer melts with the linear distribution of the monomers along the chains were found to exhibit this property independently of the composition.

The second scenario of the phase transformation involves the transitions from the isotropic phase to the bcc structure, next to the HEX-structure, and, finally, from HEX to the LAM structure. For some melts with the similar chain architecture but different compositions, the third scenario of the phase transformation takes place: the double-gyroid structure occurs on the line of the phase transformation between the hexagonal and lamellar structures. Our observation is that in the case of block copolymers ($A-B$ and $A-B-A$ melts), the G structure occurs in the melts which have significantly asymmetric compositions ($f<0.4$ and $f>0.6$). In the case of the melt with the monotonic distribution of the monomers along the chains, the G structure occurs for those distributions which deviate significantly from the linear distribution and provide notable regions of pure *A* or *B* monomers in the chain.

In all the melts which were under our consideration, we haven't found any regions of stability of the OBDD, fcc, SC, SQ, HPL, and HML structures. However, our results do not rule out a possible stabilization of the HPL and HML structures in the triblock copolymers with very asymmetric compositions ($f<0.25$). The higher harmonic corrections should be included in the theory in order to clarify this problem. We can conclude that the gradient copolymer melt is not the case of systems with stable fcc and SQ structures predicted by Marques and Cates.[33]

Despite the big differences in the single-chain architecture, the characteristic length of the ordered structures in all the melts was found to be of the same order. The peak wave-vector position of the scattering intensity of the melts with linear distribution of the monomers decreases by 5% in comparison to the melt with the diblock chain architecture. The peak wave-vector position increases for the multiblock chain architecture (2–3 blocks of the same type monomers in the chain).

We have found the regions of the stable G structure in the melts which resembled a triblock $A-B-A$ copolymer

melts with a big center block *B*. The chains with that architecture which provide such a phase property could be produced by the controlled non-steady-state polymerization reaction, since the same and smooth variation of the distribution function in both directions from the center of the chains is required.

ACKNOWLEDGMENTS

We would like to thank Dr. M. W. Matsen and Dr. W. Góźdź for valuable remarks. The help of W. Malinski and M. Sobol in arrangement of the numerical software is very appreciated. This work has been supported by KBN under Grant No. 2P03B12516.

APPENDIX

The formulas which express the vertex functions $\Gamma_n(\mathbf{q}_1,\ldots,\mathbf{q}_n)$ in terms of the momenta $S_{i,\ldots,j}(\mathbf{q}_1,\ldots,\mathbf{q}_n)=\langle\phi_i(\mathbf{q}_1),\ldots,\phi_j(\mathbf{q}_n)\rangle$ are as follows:[4]

$$\Gamma_2(\mathbf{q},-\mathbf{q})=\frac{S_{AA}(\mathbf{q})+S_{BB}(\mathbf{q})+S_{AB}(\mathbf{q})+S_{BA}(\mathbf{q})}{S_{AA}(\mathbf{q})S_{BB}(\mathbf{q})-S_{AB}(\mathbf{q})S_{BA}(\mathbf{q})}-N\chi, \tag{A1}$$

$$S_{ij}(\mathbf{q})\equiv S_{ij}(\mathbf{q},-\mathbf{q}); \tag{A2}$$

$$\begin{aligned}\Gamma_3(\mathbf{q}_1,\mathbf{q}_2,-\mathbf{q}_1-\mathbf{q}_2)&=S_{ijk}(\mathbf{q}_1,\mathbf{q}_2,-\mathbf{q}_1-\mathbf{q}_2)[S_{iA}^{-1}(\mathbf{q}_1)-S_{iB}^{-1}(\mathbf{q}_1)][S_{jA}^{-1}(\mathbf{q}_2)\\&\quad-S_{jB}^{-1}(\mathbf{q}_2)][S_{kA}^{-1}(-\mathbf{q}_1-\mathbf{q}_2)-S_{kB}^{-1}(-\mathbf{q}_1-\mathbf{q}_2)],\end{aligned} \tag{A3}$$

$$\begin{aligned}\Gamma_4(\mathbf{q}_1,\mathbf{q}_2,\mathbf{q}_3,-\mathbf{q}_1-\mathbf{q}_2-\mathbf{q}_3)&=\gamma_{ijkl}[S_{iA}^{-1}(\mathbf{q}_1)-S_{iB}^{-1}(\mathbf{q}_1)][S_{jA}^{-1}(\mathbf{q}_2)-S_{jB}^{-1}(\mathbf{q}_2)]\\&\quad\times[S_{kA}^{-1}(\mathbf{q}_3)-S_{kB}^{-1}(\mathbf{q}_3)][S_{lA}^{-1}(-\mathbf{q}_1-\mathbf{q}_2-\mathbf{q}_3)\\&\quad-S_{lB}^{-1}(-\mathbf{q}_1-\mathbf{q}_2-\mathbf{q}_3)],\end{aligned} \tag{A4}$$

$$\begin{aligned}\gamma_{ijkl}&=S_{ijm}(\mathbf{q}_1,\mathbf{q}_2,-\mathbf{q}_1-\mathbf{q}_2)S_{mn}^{-1}(-\mathbf{q}_1-\mathbf{q}_2)S_{kln}(\mathbf{q}_1+\mathbf{q}_2,\mathbf{q}_3,-\mathbf{q}_1-\mathbf{q}_2-\mathbf{q}_3)+S_{ilm}(\mathbf{q}_1,\mathbf{q}_3,-\mathbf{q}_1-\mathbf{q}_3)S_{mn}^{-1}(-\mathbf{q}_1-\mathbf{q}_3)\\&\quad\times S_{jkn}(\mathbf{q}_1+\mathbf{q}_3,\mathbf{q}_2,-\mathbf{q}_1-\mathbf{q}_2-\mathbf{q}_3)+S_{ikm}(\mathbf{q}_1,-\mathbf{q}_1-\mathbf{q}_2-\mathbf{q}_3,\mathbf{q}_2+\mathbf{q}_3)\\&\quad\times S_{mn}^{-1}(\mathbf{q}_2+\mathbf{q}_3)S_{jln}(-\mathbf{q}_2-\mathbf{q}_3,\mathbf{q}_3,\mathbf{q}_2)-S_{ijkl}(\mathbf{q}_1,\mathbf{q}_2,\mathbf{q}_3,-\mathbf{q}_1-\mathbf{q}_2-\mathbf{q}_3).\end{aligned} \tag{A5}$$

For later convenience, we introduce the following notation:

$$\Gamma_3(h,\alpha^2q^{*2})=\Gamma_3(\mathbf{q}_1,\mathbf{q}_2,-\mathbf{q}_1-\mathbf{q}_2), \tag{A6}$$

where $\mathbf{q}_1^2=\mathbf{q}_2^2=\alpha^2q^{*2}$, and $(\mathbf{q}_1+\mathbf{q}_2)^2=h\mathbf{q}_1^2$. If all the vectors in $\Gamma_4(\mathbf{q}_1,\mathbf{q}_2,\mathbf{q}_3,\mathbf{q}_4)\delta(\mathbf{q}_1+\mathbf{q}_2+\mathbf{q}_3+\mathbf{q}_4)$ belong to the same shell, then $(\mathbf{q}_1+\mathbf{q}_2)^2=h_1\mathbf{q}_1^2$, $(q_1+q_4)^2=h_2\mathbf{q}_1^2$, $\mathbf{q}_1^2=\alpha^2q^{*2}$, and

$$\Gamma_4(h_1,h_2,\alpha^2q^{*2})=\Gamma_4(\mathbf{q}_1,\mathbf{q}_2,\mathbf{q}_3,-\mathbf{q}_1-\mathbf{q}_2-\mathbf{q}_3). \tag{A7}$$

If vectors in $\Gamma_4(\mathbf{q}_1,\mathbf{q}_2,\mathbf{q}_3,\mathbf{q}_4)\delta(\mathbf{q}_1+\mathbf{q}_2+\mathbf{q}_3+\mathbf{q}_4)$ are from different shells, then let q_1 be a vector form the first shell, $\mathbf{q}_1^2=\alpha_1^2q^{*2}$, $\mathbf{q}_2^2=\alpha_2^2q^{*2}$, $\mathbf{q}_3^2=\alpha_3^2q^{*2}$, $(\mathbf{q}_1+\mathbf{q}_1)^2=h_3q^{*2}$, $(\mathbf{q}_1+\mathbf{q}_3)^2=h_4q^{*2}$, $(\mathbf{q}_1+\mathbf{q}_4)^2=h_5q$ at ^{2}, and

$$\begin{aligned}&\Gamma_4(\alpha_1^2,\alpha_2^2,\alpha_3^2,h_3,h_4,h_5)\\&\quad=\Gamma_4(\mathbf{q}_1,\mathbf{q}_2,\mathbf{q}_3,-\mathbf{q}_1-\mathbf{q}_2-\mathbf{q}_3).\end{aligned} \tag{A8}$$

The first and second shell wave vectors of the ordered structures together with the constraints imposed on phases $\phi_{k,m}$ by the symmetry group of these structures can be found elsewhere (see the references to each of the structures given in Sec. III). Below, we present coefficients $G_{xyz}^{(3)},G_{xyzp}^{(4)}$ which result from the minimization over $\phi_{k,m}$ under the constraints of a symmetry group of a given ordered structure (coefficients which are equal to zero are not presented).

LAM:

$$G_{1111}^{(4)}=6\Gamma_4(0,0,q^{*2}); \tag{A9}$$

HEX:

$$G_{111}^{(3)}=12\Gamma_3(1,q^{*2}), \tag{A10}$$

$$G_{1111}^{(4)}=18[\Gamma_4(0,0,q^{*2})+4\Gamma_4(0,1,q^{*2})]; \tag{A11}$$

SQ:

$$G_{112}^{(3)}=8\Gamma_3(2,q^{*2}), \tag{A12}$$

$$G_{1111}^{(4)}=12[\Gamma_4(0,0,q^{*2})+2\Gamma_4(0,2,q^{*2})], \tag{A13}$$

$$G_{2222}^{(4)}=12[\Gamma_4(0,0,2q^{*2})+2\Gamma_4(0,2,2q^{*2})], \tag{A14}$$

$$G_{1122}^{(4)}=8[2\Gamma_4(1,1,2,0,1,5)+\Gamma_4(1,1,2,4,1,1)]; \tag{A15}$$

SC:

$$G_{222}^{(3)}=48\Gamma_3(1,2q^{*2}), \tag{A16}$$

$$G_{112}^{(3)}=24\Gamma_3(2,q^{*2}), \tag{A17}$$

$$G_{1111}^{(4)}=18[\Gamma_4(0,0,q^{*2})+4\Gamma_4(0,2,q^{*2})], \tag{A18}$$

$$\begin{aligned}G_{2222}^{(4)}&=36[\Gamma_4(0,0,2q^{*2})+2[4\Gamma_4(0,1,2q^{*2})\\&\quad+\Gamma_4(0,2,2q^{*2})]+144\Gamma_4(1,2,2q^{*2})],\end{aligned} \tag{A19}$$

$$\begin{aligned}G_{1122}^{(4)}&=4[6(2\Gamma_4(1,1,2,0,1,5)+\Gamma_4(1,1,2,0,3,3))\\&\quad+24\Gamma_4(1,1,2,2,1,3)+6\Gamma_4(1,1,2,4,1,1)];\end{aligned} \tag{A20}$$

bcc:

$$G_{111}^{(3)}=48\Gamma_3(1,q^{*2}), \tag{A21}$$

$$G_{112}^{(3)}=24\Gamma_3(2,q^{*2}), \tag{A22}$$

$$G^{(4)}_{1111}=36[\Gamma_4(0,0,q^{*2})+2[4\Gamma_4(0,1,q^{*2}) + \Gamma_4(0,2,q^{*2})]+144\Gamma_4(1,2,q^{*2})], \quad \text{(A23)}$$

$$G^{(4)}_{2222}=18[\Gamma_4(0,0,2q^{*2})+4\Gamma_4(0,2,2q^{*2})], \quad \text{(A24)}$$

$$G^{(4)}_{1112}=144\Gamma_4(1,1,1,1,1,3), \quad \text{(A25)}$$

$$G^{(4)}_{1122}=24[2\Gamma_4(1,1,2,0,1,5)+\Gamma_4(1,1,2,0,3,3)] + 24\Gamma_4(1,1,2,4,1,1); \quad \text{(A26)}$$

fcc:

$$G^{(3)}_{112}=24\Gamma_3(\tfrac{4}{3},q^{*2}), \quad \text{(A27)}$$

$$G^{(4)}_{1111}=24[\Gamma_4(0,0,q^{*2})+6\Gamma_4(0,\tfrac{4}{3},q^{*2}) + 2\Gamma_4(\tfrac{4}{3},\tfrac{4}{3},q^{*2})], \quad \text{(A28)}$$

$$G^{(4)}_{2222}=18[\Gamma_4(0,0,\tfrac{4}{3}q^{*2})+4\Gamma_4(0,2,\tfrac{4}{3}q^{*2})], \quad \text{(A29)}$$

$$G^{(4)}_{1122}=48\Gamma_4(1,1,\tfrac{4}{3},0,1,\tfrac{11}{3})+48\Gamma_4(1,1,\tfrac{4}{3},\tfrac{8}{3},1,1); \quad \text{(A30)}$$

G:

$$G^{(3)}_{111}=48\Gamma_3(1,q^{*2}), \quad \text{(A31)}$$

$$G^{(3)}_{222}=48\Gamma_3(1,\tfrac{4}{3}q^{*2}), \quad \text{(A32)}$$

$$G^{(3)}_{112}=-24\Gamma_3(\tfrac{4}{3},q^{*2}), \quad \text{(A33)}$$

$$G^{(4)}_{1111}=24[3\Gamma_4(0,0,q^{*2})+2[6\Gamma_4(0,\tfrac{1}{3},q^{*2}) + 6\Gamma_4(0,\tfrac{2}{3},q^{*2})+6\Gamma_4(0,1,q^{*2})+3\Gamma_4(0,\tfrac{4}{3},q^{*2}) + 12\Gamma_4(0,\tfrac{5}{3},q^{*2})-6\Gamma_4(\tfrac{1}{3},\tfrac{2}{3},q^{*2}) - 6\Gamma_4(\tfrac{2}{3},\tfrac{5}{3},q^{*2})+3\Gamma_4(\tfrac{2}{3},\tfrac{8}{3},q^{*2})]], \quad \text{(A34)}$$

$$G^{(4)}_{2222}=36[\Gamma_4(0,0,\tfrac{4}{3}q^{*2})+2[4\Gamma_4(0,1,\tfrac{4}{3}q^{*2}) + \Gamma_4(0,2,\tfrac{4}{3}q^{*2})]+144\Gamma_4(1,2,\tfrac{4}{3}q^{*2})], \quad \text{(A35)}$$

$$G^{(4)}_{1112}=12[-12\Gamma_4(1,1,1,\tfrac{1}{3},\tfrac{1}{3},\tfrac{11}{3})+24\Gamma_4(1,1,1,\tfrac{1}{3},\tfrac{5}{3},\tfrac{7}{3}) - 12\Gamma_4(1,1,1,1,\tfrac{5}{3},\tfrac{5}{3})], \quad \text{(A36)}$$

$$G^{(4)}_{1122}=8[6[2\Gamma_4(1,1,\tfrac{4}{3},0,\tfrac{1}{3},\tfrac{13}{3})+\Gamma_4(1,1,\tfrac{4}{3},0,1,\tfrac{11}{3}) + 2\Gamma_4(1,1,\tfrac{4}{3},0,\tfrac{5}{3},3)+\Gamma_4(1,1,\tfrac{4}{3},0,\tfrac{7}{3},\tfrac{7}{3})] - 12\Gamma_4(1,1,\tfrac{4}{3},\tfrac{4}{3},\tfrac{1}{3},3)-12\Gamma_4(1,1,\tfrac{4}{3},\tfrac{8}{3},\tfrac{1}{3},\tfrac{5}{3})] + 48\Gamma_4(1,1,\tfrac{4}{3},4,\tfrac{1}{3},\tfrac{1}{3}); \quad \text{(A37)}$$

OBDD:

$$G^{(3)}_{111}=48\Gamma_3(1,q^{*2}), \quad \text{(A38)}$$

$$G^{(4)}_{1111}=36[\Gamma_4(0,0,q^{*2})+2[4\Gamma_4(0,1,q^{*2}) + \Gamma_4(0,2,q^{*2})]+144\Gamma_4(1,2,q^{*2})], \quad \text{(A39)}$$

$$G^{(4)}_{2222}=24[\Gamma_4(0,0,\tfrac{3}{2}q^{*2})+6\Gamma_4(0,\tfrac{4}{3},\tfrac{3}{2}q^{*2}) + 2\Gamma_4(\tfrac{4}{3},\tfrac{4}{3},\tfrac{3}{2}q^{*2})], \quad \text{(A40)}$$

$$G^{(4)}_{1122}=48[\Gamma_4(1,1,\tfrac{3}{2},0,\tfrac{1}{2},\tfrac{9}{2})+\Gamma_4(1,1,\tfrac{3}{2},0,\tfrac{5}{2},\tfrac{5}{2})] - 96\Gamma_4(1,1,\tfrac{3}{2},2,\tfrac{1}{2},\tfrac{5}{2})+24\Gamma_4(1,1,\tfrac{3}{2},4,\tfrac{1}{2},\tfrac{1}{2}); \quad \text{(A41)}$$

HML: In the case when the first shell describes a lamellar ordering, the second shell wave vectors are d times longer then the first shell ones, and

$$G^{(3)}_{112}=12\Gamma_3(1,d^2q^{*2}), \quad \text{(A42)}$$

$$G^{(4)}_{1111}=6\Gamma_4(0,0,q^{*2}), \quad \text{(A43)}$$

$$G^{(4)}_{2222}=18[\Gamma_4(0,0,d^2q^{*2})+4\Gamma_4(0,1,d^2q^{*2}), \quad \text{(A44)}$$

$$G^{(4)}_{1122}=12[\Gamma_4(1,1,d^2,0,1+d^2,1+d^2); \quad \text{(A45)}$$

HPL: The first shell describes a hexagonal ordering, and

$$G^{(3)}_{111}=12\Gamma_3(1,q^{*2}), \quad \text{(A46)}$$

$$G^{(4)}_{1111}=18[\Gamma_4(0,0,q^{*2})+4\Gamma_4(0,1,q^{*2}), \quad \text{(A47)}$$

$$G^{(4)}_{2222}=6\Gamma_4(0,0,d^2q^{*2}), \quad \text{(A48)}$$

$$G^{(4)}_{1122}=12[\Gamma_4(1,1,d^2,0,1+d^2,1+d^2). \quad \text{(A49)}$$

[1] *Surfactants in Solutions*, Vol. 1–3, edited by K. L. Mittal and D. Lindman (Plenum, New York, 1984).
[2] G. Arvidson, I. Brentel, A. Khan, G. Lindblom, and K. Fontell, Eur. J. Biochem. **152**, 753 (1985).
[3] K. Larsson, J. Phys. Chem. **93**, 7304 (1989).
[4] L. Leibler, Macromolecules **13**, 1602 (1980).
[5] *Processing, Structure, and Properties of Block Copolymers*, edited by M. J. Folkes (Elsevier, New York, 1985).
[6] F. S. Bates, Annu. Rev. Phys. Chem. **41**, 525 (1990).
[7] M. F. Schulz, A. K. Khandpur, F. S. Bates, K. Almdal, K. Mortensen, D. S. Hajdnk, and S. M. Gruner, Macromolecules **29**, 2857 (1996).
[8] P. G. de Gennes and J. Prost, *The Physics of Liquid Crystals* (Clarendon, Oxford, 1993).
[9] R. Hołyst and T. A. Vilgis, Macromol. Theory Simul. **5**, 573 (1996).
[10] G. H. Fredrickson and E. Helfand, J. Chem. Phys. **87**, 697 (1987).
[11] D. M. Anderson and E. L. Thomas, Macromolecules **21**, 3221 (1988).
[12] M. Olvera de la Cruz, Phys. Rev. Lett. **67**, 85 (1991).
[13] M. M. Disko, K. S. Liang, and S. K. Behal, Macromolecules **26**, 2983 (1993).
[14] M. W. Matsen and M. Schick, Phys. Rev. Lett. **72**, 2660 (1994).
[15] M. W. Matsen and F. S. Bates, Macromolecules **29**, 7641 (1996).
[16] M. W. Matsen and F. S. Bates, J. Chem. Phys. **106**, 2436 (1997).
[17] M. Laradji, A.-C. Shi, J. Noolandi, and R. Desai, Macromolecules **30**, 3242 (1997).
[18] I. W. Hamley and F. S. Bates, J. Chem. Phys. **100**, 6813 (1994).
[19] D. A. Hajduk, P. E. Harper, S. M. Gruner, C. C. Honeker, E. L. Thomas, and L. J. Fetters, Macromolecules **28**, 2570 (1995).
[20] D. A. Hajduk, H. Takenouchi, M. A. Hillmyer, F. S. Bates, M. E. Vigild, and K. Almdal, Macromolecules **30**, 3788 (1997).
[21] C. Yeung, A.-Ch. Shi, J. Noolandi, and R. C. Desai, Macromol. Theory Simul. **5**, 291 (1996).
[22] A. M. Mayes and M. Olvera de la Cruz, J. Chem. Phys. **91**, 7228 (1989).
[23] A. M. Mayes and M. Olvera de la Cruz, J. Chem. Phys. **95**, 4670 (1991).
[24] M. W. Matsen and M. Schick, Macromolecules **27**, 187 (1994).
[25] G. H. Fredrickson and S. T. Milner, Phys. Rev. Lett. **67**, 835 (1991).
[26] A. V. Dobrynin and L. Leibler, Macromolecules **30**, 4756 (1997).
[27] I. I. Potemkin and S. V. Panyukov, Phys. Rev. E **57**, 6902 (1998).
[28] P. J. Flory, *Principles of Polymer Chemistry* (Cornell University Press, Ithaca, 1953).
[29] H. Angerman, G. Brinke, and I. Erukhimovich, Macromolecules **29**, 3255 (1996).

[30] T. Pakula and K. Matyjaszewski, Macromol. Theory Simul. **5**, 987 (1996).
[31] S. Alexander and J. Mc Tague, Phys. Rev. Lett. **41**, 702 (1978).
[32] I. W. Hamley and V. E. Podneks, Macromolecules **30**, 3701 (1997).
[33] C. M. Marques and M. E. Cates, Europhys. Lett. **13**, 267 (1990).
[34] M. W. Matsen, Phys. Rev. Lett. **80**, 201 (1997).
[35] T. Ohta and K. Kawasaki, Macromolecules **19**, 2621 (1986).
[36] S. F. Edwards, Proc. Phys. Soc. London **88**, 265 (1966).
[37] L. D. Landau and E. M. Lifshitz, *Statistical Physics, Part 1*, 3rd ed. (Pergamon, Oxford, 1980), pp. 479.
[38] R. Hołyst and T. A. Vilgis, J. Chem. Phys. **99**, 4835 (1993).
[39] A. Aksimentiev and R. Holyst (unpublished).
[40] D. J. Amit, *Field Theory, the Renormalization Group, and Critical Phenomena* (World Scientific, Singapore, 1984), pp. 103–109.
[41] A. Aksimentiev and R. Hołyst, Macromol. Theory Simul. **7**, 447 (1998).
[42] J. L. Barrat and G. H. Fredrickson, J. Chem. Phys. **95**, 1281 (1991).
[43] W. Góźdź and R. Hołyst, Phys. Rev. Lett. **76**, 2726 (1996).
[44] W. Góźdź and R. Hołyst, Phys. Rev. E **54**, 5012 (1996).
[45] *International Tables for X-ray Crystallography*, edited by N. F. Henry and K. Lonsdale (Kynoch, Birmingham, UK, 1952), Vol. 1.
[46] R. Hołyst and W. Góźdź, *Encyclopedia of Applied Physics* (American Institute of Physics, VCH, New York, 1999) (in press).